Acta Materialia– Received 22 March 2006; received in revised form 2 August 2006; accepted 7 August 2006.

Compositional pathways and capillary effects during early-stage isothermal precipitation in a nondilute Ni-Al-Cr alloy

Chantal K. Sudbrack[1,2], Ronald D. Noebe[3] and David N. Seidman[1]*

[1]Department of Materials Science and Engineering,
Northwestern University, 2220 Campus Drive, Evanston, IL 60208 USA
[2]Argonne National Laboratory, Materials Science Division, Argonne, IL 60439 USA
[3]NASA Glenn Research Center, 21000 Brookpark Rd., Cleveland, OH 44135, USA
*Corresponding author: d-seidman@northwestern.edu, 847-491-4391

Abstract

For a Ni-5.2 Al-14.2 Cr at.% alloy with moderate solute supersaturations, the compositional pathways, as measured with atom-probe tomography, during early to later stage $\gamma'(L1_2)$-precipitation (R = 0.45-10 nm), aged at 873 K, are discussed in light of a multi-component coarsening model. Employing nondilute thermodynamics, detailed model analyses during quasi-stationary coarsening of the experimental data establish that the γ/γ' interfacial free-energy is 22-23±7 mJ m^{-2}. Additionally, solute diffusivities are significantly slower than model estimates. Strong quantitative evidence indicates that an observed γ'-supersaturation of Al results from the Gibbs-Thomson effect, providing the first experimental verification of this phenomenon. The Gibbs-Thomson relationship, for a ternary system, as well as differences in measured phase equilibria with CALPHAD assessments, are considered in great detail.

Keywords: nanostructure; coarsening; Ni alloys; atom-probe tomography; capillary phenomena

Acta Materialia– Received 22 March 2006; received in revised form 2 August 2006; accepted 7 August 2006.

I. Introduction

The precipitation process of a new phase from a supersaturated solid solution is commonly divided into a sequence of three stages: (i) nucleation of the new phase; (ii) growth of the nuclei and accompanying depletion of solute from the matrix; and (iii) coarsening (Ostwald ripening) of the precipitates of the new phase, which may operate in isolation or concurrently. In references [1-4], we report on the early-stages of isothermal, stress-free precipitation from a nondilute Ni-5.2 Al-14.2 Cr at.% alloy as monitored with transmission electron microscopy (TEM), atom-probe tomography (APT), and lattice kinetic Monte Carlo (LKMC) simulations. This work builds on the seminal research of Schmuck et al. and Pareige et al. [5,6], who were the first to demonstrate that experimental APT observations, in conjunction with LKMC simulations, yields a detailed atomic-scale picture of the early-stage decomposition of a model Ni-Al-Cr alloy. For the Ni-Al-Cr alloy that is the focus of our investigations [1-4], radial distribution function analyses of the APT data [1] demonstrate that the solutionized alloy is *not* a perfect random solid-solution. Although Cr atoms are randomly distributed in the γ(fcc)-matrix, a dispersion of congruent $L1_2$ type Ni_3Al short-range order (SRO) domains with an average radial extension of 0.6 nm results from Al diffusion during water quenching after solutionizating the alloy at temperatures above the two-phase field. As the alloy is aged at 873 K, the Al atoms in solution substitute for kinetically trapped Cr atoms in the SRO domains. The SRO processes *distinctly precede* Al-rich phase separation by nucleation of γ'($L1_2$) $Ni_3(Al_xCr_{1-x})$ precipitates, which initiates between 0.0083 and 0.167 h. During the reaction stage dominated by nucleation ($t \leq 0.25$ h), a sharp rise in the γ'-number density (N_v) of $(5.9\pm1.7)\times10^{21}$ m^{-3} s^{-1} with a constant mean precipitate radius ($\langle R \rangle$) of 0.75 nm is observed, which is an upper bound estimate for the critical γ'-radius [2]. Consistent with models of diffusion-controlled growth [7,8], the small γ'-nuclei are

Acta Materialia– Received 22 March 2006; received in revised form 2 August 2006; accepted 7 August 2006.

surrounded by a region of Al-depletion and Cr-enrichment that extends 3 nm from the γ/γ'-interface [3]. With aging from 0.25 h, the transformation enters a period of concomitant nucleation and growth that is characterized by an increasing $\langle R \rangle$ value as the rate of new nucleation events diminishes and concludes when the peak precipitate number density (N_v = 3.2×10^{24} m^{-3}) is reached after 4 h of aging [2]. The last reaction stage of concomitant growth and coarsening (t = 4-1024 h) consists of a power-law decay in N_v of –0.64±0.06 as the precipitate volume fraction, ϕ, increases. This monotonic decay in N_v, as well as the disappearance of chemical transients associated with high-order flux terms during diffusion-limited growth [3], establishes that the reaction enters quasi-stationary coarsening state after 4 h of aging, where the matrix supersaturation in the far-field changes slowly with time. A linear regression analysis of $\langle R \rangle^3$ for $t \geq 4$ h yields a coarsening rate constant of $(8.8 \pm 3.3) \times 10^{-32}$ m^3 s^{-1} and a reasonable value for $\langle R(0) \rangle$ of 0.97 nm, which is the value of $\langle R \rangle$ at which coarsening commences and it corresponds to an aging time of ca. 2 h [2]. The uniform and random distribution of coherent, spheroidal γ'-precipitates are retained out to at least 1024 h ($\langle R \rangle$ = 7.7±3.3 nm) and transformation is near its equilibrium volume fraction, ϕ^{eq}, of 15.6±0.4 %. Throughout the phase transformation, a fraction of the γ'-precipitates are interconnected by necked regions [2]. These necked regions result from early-stage coagulation and coalescence of γ'-precipitates in near proximity without significant (less than a unit cell) precipitate migration and without the formation of an anti-phase boundary in the necks, where the initial joining of the precipitates (i.e. coagulation) occurs primarily prior to 4 h of aging, and the highest percentage of interconnection (30±4 %) corresponds to the smallest interprecipitate spacing (5.9±0.8 nm).

The dependence of interfacial concentration on the curvature of the interface (i.e. a capillary effect) is addressed with classical thermodynamic Gibbs-Thomson equations for a

Acta Materialia– Received 22 March 2006; received in revised form 2 August 2006; accepted 7 August 2006.

single precipitate with a radius R (see [9]). In solid two-phase binary alloys with stress-free (i.e. negligible lattice parameter misfit) spherical precipitates, the Gibbs-Thomson effect predicts an increased solid-solubility at the interface (on both the matrix and precipitate sides of the interface) that decays as $1/R$ during isothermal aging. The product of the increase in interfacial solid-solubility for a particular phase and R value is the capillary length of that phase. This increase in solubility, and therefore the capillary length, is more pronounced in systems with high interfacial free-energies and large curvatures of the Gibbs free-energy surface of that phase. The associated compositional deviations are thought to be significant when R is less than several nanometers; that is, when the capillary lengths for both phases are ca. 0.1 nm. Due to challenges in measuring chemical composition within and across nanometer-sized precipitates these effects *have not been observed experimentally*.

The local equilibrium conditions (given by the equality of chemical potentials at the interface), which are sufficient to describe the Gibbs-Thomson effect in binary systems [10], are *insufficient* for ternary systems, as there are four concentrations that define the interfacial composition (two for each phase) but only three equilibrium conditions. An additional condition is, therefore, necessary. In the Kuehmann and Voorhees (KV) coarsening model [11], this constraint is given by the flux balance (mass conservation) at the moving precipitate/matrix interface, and Gibbs-Thompson equations are derived for a general *nonideal* and *nondilute ternary* two-phase mixture in the mean-field limit of small volume fractions. The KV model for *nondilute* coarsening in ternary alloys [11] builds on the general n-component model developed by Umantsev and Olson [12], but includes the influence of capillarity on precipitate composition. The KV model, therefore, allows both the matrix and precipitate compositions to deviate from their equilibrium values. The KV model [11] employs the following assumptions: (i) the system

Acta Materialia– Received 22 March 2006; received in revised form 2 August 2006; accepted 7 August 2006.

is in a quasi-stationary-state, that is, the matrix supersaturation changes slowly with time; (ii) the off-diagonal terms of the diffusivity matrix are negligible; (iii) the precipitates are spherical; (iv) stress effects are negligible; and (v) implicitly the evaporation-condensation mechanism is operative. Denoting the diffusivity matrix, $\overline{\overline{D_{ij}}}$, in a ternary system as:

$$\overline{\overline{D_{ij}}} = \begin{bmatrix} D_{11} & D_{12} & D_{13} \\ D_{21} & D_{22} & D_{23} \\ D_{31} & D_{32} & D_{33} \end{bmatrix}, \qquad (1)$$

the assumption that the off-diagonal terms can be neglected may be reasonable for Al, where $D_{AlAl} >> D_{AlCr}$ [13]; this assumption is, however, questionable for Cr as D_{CrCr} and D_{AlCr} are approximately the same [13]. The elastic stress effects are insignificant for the range of γ' precipitate radii we investigated (R = 0.45 to 10 nm), as governed by the small lattice parameter misfit between the γ and γ' phases (δ = 0.06±0.04 % [14]). The other assumptions of the KV model are directly addressed in the Results section.

In the limit $t \to \infty$, the exponents of the power-law temporal dependencies for an n-component system are the same as those of the LSW model (binary case) [15,16], while the coarsening rate constants for $<R(t)>$ and the γ-matrix supersaturation of solute species i (ΔC_i^{γ}), K^{KV} and $\kappa_i^{\gamma,KV}$, differ [12]. The explicit relationships derived for a ternary alloy are [11]:

$$< R(t) >^n - < R(0) >^n = K^{KV} t; \qquad (2)$$

$$N_v \cong \frac{\phi^{eq}}{4.74 K^{KV}} t^m; \text{ and} \qquad (3)$$

$$\Delta C_i^{\gamma} = < C_i^{\gamma,ff}(t) > - C_i^{\gamma,eq} = \kappa_i^{\gamma,KV} t^q; \qquad (4)$$

Acta Materialia– Received 22 March 2006; received in revised form 2 August 2006; accepted 7 August 2006.

where $n = 3$, $m = -1$, and $q = -1/3$ are the temporal exponents. The quantity $\langle R(0) \rangle$ is the mean precipitate radius at the onset of coarsening; ϕ^{eq} is the equilibrium volume fraction of the precipitates; $\langle C_i^{\gamma,ff} \rangle$ is the average far-field concentration of i in the γ-matrix; and $C_i^{\gamma,eq}$ is the equilibrium solute-solubility. In this asymptotic treatment, it is worthwhile noting that Equation 4 physically describes the $\langle C_i^{\gamma,ff} \rangle$ decay at a certain rate toward the composition of a single perfectly flat γ/γ' interface achieved at infinite time, where the latter quantity is equivalent to $C_i^{\gamma,eq}$.

Magnetic measurements of the Curie temperature were first employed in Ni-Ti alloys [17], and later in Ni-Al alloys [18,19], to determine *indirectly* the temporal evolution of the matrix supersaturation during precipitation. For γ'-strengthened Ni-Al alloys, magnetic measurements [18,19], as well as more recent direct one-dimensional atom-probe measurements [20], confirm that the matrix supersaturation of Al obeys the $t^{-1/3}$ relationship during coarsening. Recent APT investigations of the coarsening behavior in Al-Sc-X (X = Mg [21] or Zr [22]) alloys and a Ni-Al-Cr-Re [23] alloy demonstrate that the temporal dependence of the solute supersaturation agrees with or is close to ca. –1/3 for the fastest-diffusing solutes only. For the Ni-Al-Cr alloy studied, the calculated diagonal terms of the intrinsic diffusivity matrix ($^{i}D_{ij}^{fcc}$) at 873 K for the two solute species [24] (Equation 1) are close in magnitude, where $^{i}D_{AlAl}^{fcc} = 2.222\text{x}10^{-20}$ m^2 s^{-1} and $^{i}D_{CrCr}^{fcc} = 6.999\text{x}10^{-21}$ m^2 s^{-1}, and the ratio, α_D, of $^{i}D_{AlAl}^{fcc}$ to $^{i}D_{CrCr}^{fcc}$ is 3.175. During the quasi-stationary state ($t \geq 16$h), it is determined that both the power-law dependences of the Al (–0.33±0.04) and Cr supersaturations (–0.34±0.07) in the γ-matrix agree with the model value $q = -1/3$ for multicomponent coarsening [2].

Given the fine scale of the nanostructures investigated, several to hundreds of γ'-precipitates can be analyzed during an individual atom-probe tomographic (APT) analysis (with

Acta Materialia– Received 22 March 2006; received in revised form 2 August 2006; accepted 7 August 2006.

a typical analysis volume of 10x10x100 nm^3 or 100x100x100 nm^3 for the conventional tomograph or *LEAP* tomograph [25], respectively). This provides sufficient data to evaluate precisely the mean interior concentration of component *i* of the γ'-precipitates, $< C_i^{\gamma',int} >$, and the compositional profiles that extend across and into the nanometer-sized precipitates. During the reaction stage when nucleation dominations, solute-rich nuclei contain supersaturations of both Al and Cr, which are ca. 2 at.%. above the γ'-equilibrium composition, $C_i^{\gamma',eq}$ [2]. With increasing aging time, the measured solute supersaturations continuously decrease as $< C_i^{\gamma',int} >$ approaches $C_i^{\gamma',eq}$ and the γ'-precipitates' $<R>$ values increase. Compositional profile analyses established that a gradual decrease in Cr concentration towards the precipitate core that persists up to 64 h of aging is consistent with Cr atoms kinetically trapped during nucleation and growth of the γ'-precipitates [3]. In this article, we assess the origin of these solute supersaturations with the KV model. The transformation kinetics are considered in greater detail with analytical expressions developed by the KV model for the Ni-Al-Cr alloy, as was performed for Ni-Al-Mo alloys [26] and an Al-Sc-Mg alloy [21,27]. From our APT measurements [2], the γ/γ' interfacial energy, $\sigma^{\gamma/\gamma'}$, and effective solute diffusivities are determined using ideal dilute-solution theory and CALPHAD assessments [28,29] of the nonideal and nondilute thermodynamics of the γ- and γ'-phases employing the KV model.

II. Experimental Procedures

High purity constituent elements (99.97 Ni wt. %, 99.98 Al wt. %, and 99.99 Cr wt. %) were induction melted under an Ar atmosphere to minimize oxidation, and then chill cast in a 19 mm diam. copper mold to produce master ingots. The overall alloy composition, C_i^o, was determined to be 80.5_2 Ni-5.2_4 Al-14.2_4 Cr at. % employing inductively coupled plasma atomic-

Acta Materialia– Received 22 March 2006; received in revised form 2 August 2006; accepted 7 August 2006.

emission spectroscopy. To ensure chemical homogeneity, cast ingots, consisting of coarse (0.5–2 mm diam.), equiaxed, and twinned grains [14], were homogenized at 1573 K for 24 hours. Subsequently, the temperature was decreased to 1123 K and the ingot was held for 3 h in the γ(fcc)-phase field. By virtue of the smaller undercooling, this heat treatment reduced the concentration of quenched-in vacancies and suppressed γ'($L1_2$)-precipitation during the water quench to room temperature. As-quenched sections were aged at 873 K for times ranging from 0.0333 to 1024 h. Further details on sample preparation, operational conditions and measurements for APT and transmission electron microscopy (TEM) experiments can be found in references [2,14,23]. APT data was visualized and analyzed with ADAM 1.5 [30], where the γ/γ' interfaces are delineated with 9 at.% Al isoconcentration surfaces generated with efficient sampling procedures [31] and the composition profiles are obtained with the proximity histogram method [32].

III. Results

3.1. Experimental observations of supersaturation and equilibrium and nonequilibrium composition of the γ and γ' phases

Figure 1 presents a typical 3-dimensional image that is obtained with APT for a specimen aged for 4 h at 873 K. Over the reaction period investigated, the fine-scale nanostructure exhibits some coalescence among the uniform distribution of spheroidal γ'-precipitates. Figures 2 displays the temporal evolution of the far-field composition in the γ-matrix, $< C_{Ni}^{\gamma,ff} >$ with time as supersaturation is relieved. Following Marquis and Seidman [21,27], the equilibrium composition and compositional rate constants of the matrix phase are deduced from the experimental measurements of $< C_i^{\gamma,ff} >$ in quasi-stationary state $t \geq 16$ h with Equation 4 assuming the model p value of –1/3. The fit to Equation 4 is marked with solid lines in Figure 2,

Acta Materialia– Received 22 March 2006; received in revised form 2 August 2006; accepted 7 August 2006.

where the extrapolation of the fitted curves to shorter aging times is denoted with dashed lines. This fitting procedure yields a goodness of fit of 70% or better for each *i*. The extrapolated values for $C_i^{\gamma,eq}$ for Al and Cr are 3.13±0.04 and 15.61±0.09 at.%, respectively, while the Al and Cr rate constants are determined to be 0.186±0.022 and –0.14±0.05 at.fr. $s^{1/3}$, respectively. The law of mass conservation mandates that the relationship in Equation 4 also obtains for the solvent Ni, thus providing a veracity check for the fitting procedure used. From the experimental measurements of $< C_{Ni}^{\gamma,ff} >$ (Figure 2), the $C_{Ni}^{\gamma,eq}$ value is 81.26±0.09 at.%, satisfying mass conservation, since the sum of the concentrations of Ni, Al and Cr in the γ-phase is 100.00±0.11 at.%.

In the KV [11] analysis, they derive a Gibbs-Thomson relationship (*see* Equations 16 and 17 for each solute species in their article) that describes the influence of interfacial curvature *on precipitate composition* for a coarsening spherical precipitate of radius R in a ternary alloy. For the γ'-phase, in the asymptotic limit when *both* solute supersaturations decay as $t^{-1/3}$, and assuming $\langle R \rangle \approx R$, it can be shown that their Equations 16 and 17 simplifies to:

$$< C_i^{\gamma'}(t) > - C_i^{\gamma',eq} = \kappa_i^{\gamma',KV} t^{-1/3}; \qquad (5)$$

where $\kappa_i^{\gamma',KV}$ is a compositional rate constant; $< C_i^{\gamma',int}(t) >$ is the average precipitate concentration in their interiors; and $C_i^{\gamma',eq}$ is the precipitate composition at a flat interface, which is equal to the equilibrium value of the precipitate composition. Analogously to the γ-matrix phase, the $< C_i^{\gamma',int}(t) >$ values for the γ'-precipitates are fit to Equation 5, yielding $C_i^{\gamma',eq}$ and $\kappa_i^{\gamma'}$ values with a goodness of fit of 70% or better (Figure 3). To obtain more precise values for the quantities $C_i^{\gamma',eq}$ and $\kappa_i^{\gamma',KV}$ the $< C_i^{\gamma',int}(t = 4\ h) >$ value was included with the quasi-stationary-state values ($t \geq 16$ h) in the fitting. The latter's inclusion is reasonable, since the temporal exponent for $\langle R(t) \rangle^n - \langle R(0) \rangle^n$ (Equation 2) is 0.29±0.05 for $t \geq 1$ h (in reasonable agreement

Acta Materialia– Received 22 March 2006; received in revised form 2 August 2006; accepted 7 August 2006.

with the model prediction of n=1/3) and a linear monotonic decay of N_v is observed for $t \geq 4$ h [2].

As seen in Figure 3, the γ'-precipitates' cores are supersaturated with Al (19.1±2.8 at.%) and Cr (9.7±2.1 at.%) at t = 0.167 h. These supersaturations in the γ'-precipitates decrease continuously and the measured $< C_i^{\gamma',int} >$ is 16.70±0.29 at.% Al and 6.91±0.20 at.% Cr at t = 1024 h. Utilizing Equation 5, the extrapolated values for the $C_i^{\gamma',eq}$ values of Ni, Al, and Cr are 76.53±0.25, 16.69±0.22, and 6.77±0.15% at.%, respectively, while the $\kappa_i^{KV,\gamma'}$ values are –0.48±0.13, 0.22±0.11, and 0.26±0.08 at.fr. $s^{1/3}$, respectively. The excess or deficiency of solute with respect to the equilibrium compositions, that is, the supersaturation, is summarized for both phases as a function of $<R>$ and aging time in Table 1. Table 2 lists the rate constants and the equilibrium phase compositions determined independently from the measured concentrations of each component as they evolve temporally. In both phases, conservation of mass flux constrains the summation of the elemental rate constants to zero. Within experimental error, the independent measurements of the rate constants sums to zero, thereby confirming that the fitting procedures are reasonable.

3.2. Comparison of APT measurements to calculated values based on CALPHAD thermodynamic assessments

The Ni-Al-Cr system [28,33] and commercial Ni-base superalloys [29] have been the subject of a number of CALPHAD thermodynamic assessments, accessible from the commercial software package *ThermoCalc* [34]. Standard *ThermoCalc* procedures were employed to calculate an equilibrium state for Ni-5.24 Al-14.24 Cr at.% (C_i^o) at a constant pressure (1 atm) and 873 K. Table 3 contains a comparison of the APT measurements of the γ'-equilibrium

Acta Materialia– Received 22 March 2006; received in revised form 2 August 2006; accepted 7 August 2006.

volume fraction (ϕ^{eq}), the composition of the critical nucleus ($C_i^{\gamma',*}$), $C_i^{\gamma',eq}$ and $C_i^{\gamma,eq}$ with calculated values from the thermodynamic databases. The value of ϕ^{eq} is determined directly with APT from $C_i^{\gamma,eq}$ and $C_i^{\gamma',eq}$ of each component using the lever-rule, $\phi_{LR}^{eq} = \left(C_i^{\gamma,eq} - C_i^{o}\right)/\left(C_i^{\gamma,eq} - C_i^{\gamma',eq}\right)$, to have an average value of 15.6 % (Table 3). For a specimen aged for 1024 h, the ϕ-value measured directly from the APT analyzed volumes is 15.6±6.4 at.% [2], establishing that the transformation is near completion. The thermodynamic assessments predict lower values of ϕ^{eq} than the experimental values with 7.49 at.%, 12.34 at.%, and 12.83 at.% predicted by Huang and Chang's [33], Dupin et al.'s [28], and Saunders' [29] databases, respectively. As the Dupin et al. and Saunders databases yield reasonable values of ϕ^{eq} when compared to our experimental value, only the calculated compositional quantities of these two databases are listed in Table 3, and these databases are used to calculate the thermodynamic quantities needed to analyze data with the KV model. The database of Huang and Change is *not* considered further as it is not in agreement with the experimental value of ϕ^{eq}.

Thermodynamic assessment predictions for the equilibrium composition of the γ-matrix are near the experimental values, although the experimental values are slightly more depleted in Al (3.13±0.04 at.%) and enriched in Cr (15.61±0.09 at.%) than predicted. The agreement is not as close for the γ'-phase. From phase-equilibria, the $C_i^{\gamma',*}$ value, as well as the driving force for γ'-nucleation, can be calculated from the common tangent plane between the initial composition on the γ-matrix free-energy surface with the γ'-precipitates' free-energy surface. In agreement with the thermodynamic database predicted trends, the critical γ'-nucleus is observed to be supersaturated with Al (18.3±0.9 at.%) above the Al solvus concentration (16.69±0.22 at.%) at a supersaturation of 1.61 at.%, similar to the predicted Al supersaturations of 1.81 at.% [28] and

Acta Materialia– Received 22 March 2006; received in revised form 2 August 2006; accepted 7 August 2006.

1.19 at.% [29]. The observed critical γ'-nuclei are highly depleted in Ni, ca. 4 at.%, relative to the experimental $C_{Ni}^{\gamma',eq}$, while assessments predict significantly smaller deviations (< 0.25 at.%). This high Ni depletion, where $< C_{Ni}^{\gamma',int} >$ = 72.4±1.1 at.%, most likely results from fast Al diffusion during the quench from the solutionizing temperature, 1123 K, which produces a distribution of Ni_3Al-type $L1_2$ SRO domains in the as-quenched alloy [1]. The most striking discrepancy between the experiments and the CALPHAD predictions is the Cr concentrations in the γ'-phase. Contrary to the predicted trend of $C_{Cr}^{\gamma',*} < C_{Cr}^{\gamma',eq}$, it is found that critical nuclei contain ca. 2.5 at.% of Cr *above* the $C_{Cr}^{\gamma',eq}$ value. For the discussed *binary* Gibbs-Thomson formulation, the observed trend requires the curvature of the Gibbs free-energy surface of the γ'-phase to be negative, which is inconsistent with a positive curvature needed for thermodynamic stability. In a ternary alloy, the thermodynamic description, however, is less straightforward and the Gibbs-Thomson relationship depends on three curvatures [11]. In reference [3] we show that Cr atoms are kinetically trapped in the nucleating γ'-precipitates; the observed trend is therefore a kinetic effect that is not described by thermodynamics and assessments based on thermodynamics such as the CALPHAD approach.

IV. Discussion

1. *Determination of γ/γ' interfacial free-energy and solute diffusivities*

The coarsening rate constant, K^{KV}, Equations 2 and 3, for the temporal evolution of the precipitate radius in a γ plus γ' ternary alloy is given by [11]:

$$K^{KV} = \frac{8\sigma^{\gamma/\gamma'} V_m^{\gamma'}}{9\Lambda}; \qquad (7)$$

Acta Materialia– Received 22 March 2006; received in revised form 2 August 2006; accepted 7 August 2006.

where $V_m^{\gamma'}$ is the average atomic volume per mol of the γ'-precipitate phase; $\sigma^{\gamma/\gamma'}$ is the γ/γ' interfacial free energy. The coefficient Λ contains thermodynamic and kinetic information for the alloy as given by:

$$\Lambda = \frac{p_{Al}}{D_{AlAl}}\left(p_{Al}G^{\gamma}_{,AlAl} + p_{Cr}G^{\gamma}_{,AlCr}\right) + \frac{p_{Cr}}{D_{CrCr}}\left(p_{Al}G^{\gamma}_{,AlCr} + p_{Cr}G^{\gamma}_{,CrCr}\right); \tag{8}$$

where $G^{k}_{,ij}$ is shorthand notation for the partial derivatives of the molar Gibbs free-energy of phase k as given by:

$$G^{k}_{,i,j} = \frac{\partial G(k)}{\partial C_i \partial C_j}. \tag{9}$$

The quantity p_i is the magnitude of the partitioning as defined by $p_i = C_i^{\gamma',eq} - C_i^{\gamma,eq}$. While, the compositional rate constant, $\kappa_i^{\gamma,KV}$, for the evolution of the γ-matrix solute supersaturation for a ternary alloy during quasi-stationary coarsening is [11]:

$$\kappa_i^{\gamma,KV} = \frac{\left(3\sigma^{\gamma/\gamma'}V_m^{\gamma'}\right)^{2/3}\Lambda^{1/3}p_i}{p_{Al}\left(p_{Al}G^{\gamma}_{,AlAl} + p_{Cr}G^{\gamma}_{,AlCr}\right) + p_{Cr}\left(p_{Al}G^{\gamma}_{,AlCr} + p_{Cr}G^{\gamma}_{,CrCr}\right)}. \tag{10}$$

There are different models accounting for diffusional field overlap associated with systems with nonzero volume fractions; see reference [9] for an overview of this problem. The restriction of small volume fractions can be removed by substituting $K(\phi)$ into Equations 2 and 4 with:

$$K(\phi) = f(\phi)K^{KV}; \text{ and} \tag{11}$$

$$\kappa_i^{\gamma}(\phi) = \left(f(\phi)\right)^{-1/3}\kappa_i^{\gamma,KV}; \tag{12}$$

where $f(\phi)$ is the ratio of the finite volume fraction rate constant to the rate constant of the KV model, $K(\phi)/K^{KV}$. The values of $f(0.156)$ for six different models vary over a small range (1.65 –

Acta Materialia– Received 22 March 2006; received in revised form 2 August 2006; accepted 7 August 2006.

2.35) [9,35] and Brailsford's and Wynblatt's [36] theoretical value of 2.3 is chosen as being representative.

By measuring independently the coarsening rate constants for <*R*> and the evolution of the average concentration of solute in the matrix, it is possible to determine the interfacial free-energy and the solute diffusivity, independently of one another, as first shown by Ardell [18,19] for a binary alloy, and later for a ternary alloy by Marquis and Seidman [21,27]. Utilizing Equations 7– 12, the relationship for $\sigma^{\gamma/\gamma'}$ in a nonideal, nondilute γ plus γ' ternary alloy *with a finite volume fraction* is given by:

$$\sigma_i^{\gamma/\gamma'} = \frac{\left(K^{KV}\right)^{1/3}\kappa_i^{\gamma,KV}}{2V_m^{\gamma'}p_i}\left(p_{Al}{}^2G^{\gamma}_{,AlAl} + 2p_{Al}p_{Cr}G^{\gamma}_{,AlCr} + p_{Cr}{}^2G^{\gamma}_{,CrCr}\right). \tag{13}$$

The measured Al diffusion coefficient (diagonal term), $D_{AlAl}^{eff,i}$, is an effective measure of the operating diffusional processes, as determined from either $\kappa_i^{\gamma,KV}$ for solute species i and it is given by:

$$D_{AlAl}^{eff,i} = \frac{9\left(K^{KV}\right)^{2/3}p_i}{4\kappa_i^{\gamma,KV}f(\phi)}\cdot\frac{\left(p_{Al}{}^2G^{\gamma}_{,AlAl} + (1+\alpha_D)p_{Al}p_{Cr}G^{\gamma}_{,AlCr} + p_{Cr}{}^2G^{\gamma}_{,CrCr}\right)}{\left(p_{Al}{}^2G^{\gamma}_{,AlAl} + 2p_{Al}p_{Cr}G^{\gamma}_{,AlCr} + p_{Cr}{}^2G^{\gamma}_{,CrCr}\right)}; \tag{14}$$

where the constraint α_D (the ratio of solute diffusivities) is taken to be 3.175 based on the calculated intrinsic diffusivities. For the special case when one solute diffusivity is much greater than the other, a simplified expression that removes this constraint can be derived [21,27]. It follows from Equation 14 that an average $D_{AlAl}^{eff,i}$ based on the compositional evolution of both solute species is:

$$< D_{AlAl}^{eff} >= \frac{9\left(K^{KV}\right)^{2/3}\left(p_{Al}+p_{Cr}\right)}{4\left(\kappa_{Al}^{\gamma,KV}+\kappa_{Cr}^{\gamma,KV}\right)f(\phi)}\cdot\frac{\left(p_{Al}{}^2G^{\gamma}_{,AlAl} + (1+\alpha_D)p_{Al}p_{Cr}G^{\gamma}_{,AlCr} + p_{Cr}{}^2G^{\gamma}_{,CrCr}\right)}{\left(p_{Al}{}^2G^{\gamma}_{,AlAl} + 2p_{Al}p_{Cr}G^{\gamma}_{,AlCr} + p_{Cr}{}^2G^{\gamma}_{,CrCr}\right)}; \tag{14b}$$

Acta Materialia– Received 22 March 2006; received in revised form 2 August 2006; accepted 7 August 2006.

where $< D^{eff}_{CrCr} >$ is determined directly from the constraint condition, $< D^{eff}_{AlAl} >= 3.175 < D^{eff}_{CrCr} >$. It is important to note that after algebraic rearrangement $f(\phi)$ is not present in Equation 13; while it is present in Equation 14.

To determine $\sigma^{\gamma/\gamma'}$ and $D^{eff,i}_{AlAl}$ from Equations 13 and 14 requires that the molar Gibbs free-energy of the γ-matrix be known. For the general case described by nonideal and nondilute solution theory, such as the alloy discussed herein, CALPHAD methods can be employed to calculate the $G^k_{,ij}$ at a given composition. Table 4 presents $G^{\gamma}_{,ij}$ and $G^{\gamma'}_{,ij}$ for two thermodynamic assessments [28,29], and $G^{\gamma}_{,ij}$ for the ideal solution evaluated at the solvus compositions. For the free-energy of the γ-matrix evaluated at $C^{\gamma,eq}_i$, the two CALPHAD assessments predict $G^k_{,ij}$ with similar magnitudes. They predict, however, a more highly curved free-energy surface than ideal solution theory with respect to all solute species combinations. To determine $\sigma^{\gamma/\gamma'}$ and $D^{eff,i}_{AlAl}$ from Equations 13 and 14, $V^{\gamma'}_m$ is defined as $N_A(a^{\gamma'})^3/4$, where $a^{\gamma'}$ is the lattice parameter of the γ'-phase (0.3554 nm [37]) and N_A is Avogadro's number, yielding $V^{\gamma'}_m = 6.7584\text{x}10^{-6}$ m^3 mol^{-1}. Table 5 displays the $\sigma^{\gamma/\gamma'}_i$ calculated from the experimental values of $K^{KV} = (8.8\pm3.3)\text{x}10^{-32}$ m^3 s^{-1} and $\kappa^{\gamma,KV}_I$ (Table 2) employing Equation 13, with the calculated $G^{\gamma}_{,ij}$ (Table 4) and measured equilibrium compositions (Table 3). The CALPHAD assessments take into account the excess free-energies of mixing and the magnitudes of $G^{\gamma}_{,ij}$ and are 1.5 to 12 times larger than those for ideal solution theory (Table 4). Interestingly, both the CALPHAD assessments and ideal solution theory yield approximately the same value for $\sigma^{\gamma/\gamma'}_i$, 22-23±7 mJ m^{-2}. Equation 13 consists of a constant prefactor term multiplied by a polynomial term (in parenthesis) that depends on $G^{\gamma}_{,ij}$ (always > 0) and p_i. For the alloy under investigation, two terms of the polynomial are greater than 0, as both p_{Al}^2 and p_{Cr}^2 are greater than 0, and one term is less than 0, since $p_{Al}p_{Cr}$ is less than 0. The

Acta Materialia– Received 22 March 2006; received in revised form 2 August 2006; accepted 7 August 2006.

calculated individual terms in the polynomial do differ significantly between ideal solution theory values and CALPHAD assessments; however, the sum of negative and positive contributions yields polynomial values that are in near agreement. The calculated polynomial values are 4612, 5025, and 4794 J mol^{-1} at.fr.^{2} for ideal solution theory, Dupin et al.'s database, and Saunders' database, respectively, which differ within 9% of each other and yield values in near agreement for $\sigma_i^{\gamma/\gamma'}$.

A model prediction of the coarsening rate constant for $\langle R \rangle$, $K(\phi)$, is determined from Equation 11 (using Equations 7-8) to be 1.29×10^{-30} m^3 s^{-1}, utilizing the calculated intrinsic diffusivities (Table 6) and an interfacial free-energy of 22.5 mJ m^{-2}. The calculated $K(\phi)$ is approximately 15 times larger than the measured rate constant of $(8.8 \pm 3.3) \times 10^{-32}$ m^3 s^{-1}, which implies that the experimental coarsening kinetics are significantly *slower* than the model predictions. Correspondingly, as seen in Table 6, the effective solute diffusivities determined by Equations 14 and 14b, are one order of magnitude smaller than the predicted intrinsic diffusivities *in the matrix phase*. The smaller rate is attributed to diffusion occurring *in both the* γ *and* γ'*-phases* [2], where tracer Al and Cr diffusivities at 873 K in pure Ni_3Al are 2.7×10^{-23} m^2 s^{-1} [38] and 1.4×10^{-23} m^2 s^{-1} [39], respectively.

2. *The influence of capillarity on the* γ'*-precipitate composition*

The Ni-rich corner of the equilibrium Ni-Al-Cr phase diagram at 873 K and calculated tie-lines presented in Figure 4 were calculated with *ThermoCalc* employing the two thermodynamic assessments [28,29]. Equilibrium concentration predictions by *ThermoCalc* are largely based on an empirical fitting to available experimental data. The Ni-Al-Cr system has been extensively studied experimentally between 1023 to 1123 K [37], while at 873 K phase

Acta Materialia– Received 22 March 2006; received in revised form 2 August 2006; accepted 7 August 2006.

equilibria data is limited. Therefore, the thermodynamic assessments at 873 K yield calculated quantities that are approximate. As seen in Figure 4, an experimental tie-line, deduced directly from the APT compositional measurements, differs significantly from the calculated tie-lines, which, indicates the inability of the extant thermodynamics assessments to account adequately the final equilibrium state. The Dupin et al. database gives a better γ'/(γ'+γ) solvus curve than does the Saunders et al. database, while the inverse is true for the (γ'+γ)/γ. The inclusion of a capillary effect on the γ'-precipitate composition in the KV model leads to the prediction that the trajectory of the γ-matrix composition must lie along the tie-line, while the γ'-precipitate's trajectory does *not*. As shown in Figure 4, our experimental results provide the first experimental verification of this effect, where $< C_i^{\gamma,ff} >$ and $< C_i^{\gamma',int} >$ values are plotted employing open triangles and open diamonds, respectively. The γ'-precipitate's trajectory clearly does not follow the tie-line. The slope of the matrix trajectory is predicted by the KV model to be the ratio of the difference in elemental partitioning, p_2/p_3. The measured slope of the matrix trajectory is 1.53±0.05, and is close to the predicted slope of p_{Al}/p_{Cr} = 1.36±0.10, from the extrapolated equilibrium phase compositions. To test if the origin of this behavior is due to capillarity, the measured solute supersaturations in γ'-precipitates (Table 2) are compared to the calculated predictions below.

In the alloy under investigation, the γ'-precipitates exhibit an enhanced solid-solubility of Al and Cr that decays with time (Figure 3). In reference [3], it is shown that the Cr enhancement results from kinetically trapped Cr atoms in the nucleation and growth of γ'-precipitates, leading to a gradient in Cr concentration within the γ'-precipitates. While, the Al concentration within the γ'-precipitates, even after the shortest aging times, has a constant plateau concentration throughout the core. The decay of the Al supersaturation with time, as the precipitates grow, may

Acta Materialia– Received 22 March 2006; received in revised form 2 August 2006; accepted 7 August 2006.

result from capillarity, which, for ternary systems, can be tested using the Gibbs-Thomson relationship for the precipitate [11]. The magnitude of this effect depends strongly on the solution thermodynamics of both phases, $\sigma^{\gamma/\gamma'}$, and R, and for a single precipitate in a nonideal and nondilute ternary alloy the supersaturation is given by [11]:

$$\Delta C_i^{\gamma'} = < C_i^{\gamma'}(t) > - C_i^{\gamma',eq} = \frac{2\sigma^{\gamma/\gamma'}\left(\overline{V_{Ni}^{\gamma'}}\eta_{Ni}^i + \overline{V_{Al}^{\gamma'}}\eta_{Al}^i + \overline{V_{Cr}^{\gamma'}}\eta_{Cr}^i\right)}{\left(G_{,AlAl}^{\gamma'}G_{,CrCr}^{\gamma'} - \left(G_{,AlCr}^{\gamma'}\right)^2\right)\Lambda}\frac{1}{R}$$
$$- \frac{\left(p_{Al}G_{,iAl}^{\gamma'} + p_{Cr}G_{,iCr}^{\gamma'}\right)\left(G_{,AlAl}^{\gamma}G_{,CrCr}^{\gamma} - \left(G_{,AlCr}^{\gamma}\right)^2\right)}{\left(G_{,AlAl}^{\gamma'}G_{,CrCr}^{\gamma'} - \left(G_{,AlCr}^{\gamma'}\right)^2\right)\Lambda}\cdot$$
$$\left(\frac{p_{Cr}}{D_{CrCr}}\left(< C_{Al}^{\gamma,ff}(t) > - C_{Al}^{\gamma,eq}\right) - \frac{p_{Al}}{D_{AlAl}}\left(< C_{Cr}^{\gamma,ff}(t) > - C_{Cr}^{\gamma,eq}\right)\right) \quad (15)$$

Where $\overline{V_i^{\gamma'}}$ is the molar volume of component i in the γ'-precipitate phase, the coefficient Λ is defined by Equation 8, and the six coefficients η_j^i of a form similar to Λ, are defined in an Appendix to reference [11]. Unlike the case of a binary alloy, this Gibbs-Thomson relationship contains two terms, where the first-term decays as $1/R$.

The curvatures of the Gibbs free-energy surfaces for the γ-phase and γ'-phase are calculated using the Dupin et al. [28] and Saunders [29] thermodynamic databases for Ni-base alloys (Table 4). Unlike the γ-phase, where the two databases are in near agreement at the equilibrium composition, the Saunders database predicts large curvatures in the Gibbs free-energy surface for the γ'-phase, while the Dupin et al. database predicts curvatures of similar magnitude to those of the γ-phase. For the γ-phase, since the curvature predictions of both databases are nearly equivalent, they yield approximately the same value (~22.5 mJ m^{-2}) for the

Acta Materialia– Received 22 March 2006; received in revised form 2 August 2006; accepted 7 August 2006.

γ/γ' interfacial free-energy (Table 5) determined from the rate constants for R and ΔC_i^{γ} using Equation 13.

For ternary systems, Equation 15, unlike the analogous equation for the binary case, *contains a second term*, denoted $\Delta C_i^{II\gamma'}$, which is a function of the time-dependent solute concentrations in the far-field region of the matrix-phase. To determine the overall contribution of this term to the power-law temporal dependence of the Al supersaturation with <*R*>, $\Delta C_{Al}^{II\gamma'}$ is calculated from $< C_{Al}^{\gamma,ff}(t) > - C_{Al}^{\gamma,eq}$ at each aging time with the measured solute diffusivities, $< D_{AlAl}^{eff} >$ and $< D_{CrCr}^{eff} >$ (Table 6). It is plotted on a double logarithmic plot versus <*R*> in Figure 5. Since the relationship in Equation 15 depends on R, and not t, $\Delta C_i^{\gamma'}$ is affected by *the ratio* of the two solute diffusivities, α_D; that is, for a constant α_D-value (independent of diffusivities' magnitudes), Equation 15 yields equivalent $\Delta C_i^{\gamma'}$ values. Figure 5 demonstrates that the contribution of the second term to the Al supersaturation is small for the Ni-Al-Cr alloy studied, but not insignificant for the smallest precipitates evaluated with the Saunders database. Where the quantity $\Delta C_{Al}^{II\gamma'}$ is ca. 0.15 at.% at an <*R*> value of 1 nm, while for the Dupin et al. database, $\Delta C_{Al}^{II\gamma'}$ is ca. 0.03 at.% at the same <*R*> value. The higher values of $\Delta C_{Al}^{II\gamma'}$ determined from the Saunders database evaluation results from the larger free-energy curvatures for the γ'-phase, as $\Delta C_{Al}^{II\gamma'}$ is directly proportional to $\left(p_{Al}G_{,iAl}^{\gamma'} + p_{Cr}G_{,iCr}^{\gamma'}\right)$. This suggests that the second term may make a significant contribution to the supersaturation in the precipitates when the precipitate phase's free-energy surface is highly curved.

Figure 6 exhibits the experimental measurements of $\Delta C_{Al}^{\gamma'}$ compared to the predictions of Equation 15 (including $\Delta C_{Al}^{II\gamma'}$) using the Dupin et al. and Saunders thermodynamic databases. Exceptionally good agreement is found between the experimental data and the prediction of the

Acta Materialia– Received 22 March 2006; received in revised form 2 August 2006; accepted 7 August 2006.

KV model employing the Dupin et al. database. This result provides unequivocal proof that the enhancement of Al solubility in the γ'-precipitates with decreasing <*R*> results from capillarity. Furthermore, the agreement suggests a shallow free-energy surface for the γ'-phase, as predicted by the Dupin et al. database, is appropriate for the γ'-phase in Ni-5.2 Al-14.2 Cr at.% at 873 K. To the best of our knowledge, this is the first experimental verification of this aspect of the capillary effect in the solid-state. And it has been obtained from direct compositional measurements of nanometer-sized precipitates employing APT.

As seen in Table 1, the measured $\Delta C_{Cr}^{\gamma'}$-values are slightly larger than the measured $\Delta C_{Al}^{\gamma'}$-values. Since the thermodynamic assessments incorrectly predict the behavior of the Cr supersaturations, a similar analysis for Al supersaturations cannot be applied to Cr. The temporal behavior with respect to <*R*> can, however, be evaluated. Figure 7a presents a double logarithmic plot of $\Delta C_{Cr}^{\gamma'}$ versus <*R*>. For aging times in the quasi-stationary-state ($t \geq 16$ h), the temporal power-law of t^{-1} (solid-line) fits the experimental measurements with a goodness fit of 95% consistent with general trend for capillarity. As seen from the extrapolation of this fit (dotted-line), the measured $\Delta C_{Cr}^{\gamma'}$ values at shorter aging times are slightly higher than the fit's prediction, which, like $\Delta C_{Al}^{\gamma'}$, may result from a non-negligible $\Delta C_{Cr}^{II\,\gamma'}$ term for <*R*> ≤ 1.27 nm. As a comparison, Figure 7b presents the negative $\Delta C_{Cr}^{\gamma'}(< R >)$ values predicted by the thermodynamic assessments as determined from Equation 15, when $\Delta C_{Cr}^{II\,\gamma'}$ is assumed to be zero. As is the case for Al, the Dupin et al. assessment (dashed line) predicts a larger Cr supersaturation due to a more shallow γ'-free energy surface. We emphasize that the observed trend in Cr supersaturation is a direct result of kinetically trapped Cr atoms for aging times up to 64 h [3].

Acta Materialia– Received 22 March 2006; received in revised form 2 August 2006; accepted 7 August 2006.

V. Summary and Conclusions

We present detailed results and analyses that both supplement and complement those reported in reference [2] on atom-probe tomography (APT) measurements of the nanostructural and compositional evolution in a low to moderate supersaturated Ni-5.2 Al-14.2 Cr at. % model superalloy undergoing a first-order isothermal (873 K) phase transformation, γ(fcc) → γ(fcc) plus γ'($L1_2$) leading to the following results and conclusions:

- The coarsening kinetics of the γ'-precipitates, with measured radii ranging from 0.45 to 10 nm, are analyzed with a coarsening model for a ternary alloy developed by Kuehmann and Voorhees (KV) (Equations 2-15) that includes capillary effects on precipitate composition. The KV model is based on a general model of an n-component alloy without capillarity [12], applicable to nonideal and nondilute systems with near-zero volume fraction. The KV model is modified [36] to incorporate the influence of a finite volume fraction to obtain coarsening rate constants (Equations 11 and 12) and solute diffusivity (Equations 14 and 14b), where the measured equilibrium γ'-volume fraction is 15.6%, Table 3.

- Extrapolations based on Equations 2 and 5 from the measured γ-matrix far-field and γ'-precipitate core compositions to $t = \infty$ permit the equilibrium solvus line compositions to be determined (Table 3). Compared to CALPHAD predictions based on two thermodynamic databases [28,29], which predict reasonably the γ'-equilbrium volume fraction, our extrapolated solvus and measured critical radius compositions differ (Table 3). The experimental measured critical radius composition is 72.4±1.1 Ni-18.3±0.9 Al-9.3±0.7 Cr at.% at a radius of 0.75 nm.

Acta Materialia– Received 22 March 2006; received in revised form 2 August 2006; accepted 7 August 2006.

- The composition trajectory of the γ-matrix (Figure 4) follows the experimental tie-line with a slope of –1.36±0.36, while the trajectory of the γ'-precipitate composition does *not* follow the tie-line, thereby providing the first experimental evidence of this behavior predicted by the KV model for ternary systems whose decomposition behavior is influenced by capillary effects.

- Using the experimentally determined rate constants for the average precipitate radius [$(8.8\pm3.3)\times10^{-32}$ m^3 s^{-1}] and the matrix supersaturation (Table 2), the interfacial free-energy and the effective diffusion coefficients of Al and Cr are determined independently of one another (Tables 6 and 7). The γ/γ' interfacial free-energy is (22-23)±7 mJ m^{-2} for ideal solution thermodynamics and thermodynamics based on CALPHAD assessments (Table 5), respectively. The observed kinetics are slower than what is predicted by the KV model, which is attributed to non-negligible slower diffusivities within γ'-precipitates than matrix diffusivities to the overall diffusional processes. Accordingly, the effective diffusivities are 15 times smaller than the calculated matrix diffusivities (Table 6).

- The expression for the Gibbs-Thomson relationship in the precipitate phase derived by the KV model for a ternary system contains two terms, where the first decays as $1/R$ (Equation 15). This relationship is evaluated in detail for the temporal evolution of the measured Al supersaturation in γ'-precipitates (Table 1) in Figures 7 and 8. The second-term in Equation 15 is found to contribute less than tenths of an at.% to the overall Al supersaturation (Figure 5) and a detailed analysis provides strong evidence that the observed supersaturation is due to capillarity. In contrast to predictions by CALPHAD thermodynamic assessments, the γ'-precipitates (Table 1) are supersaturated with Cr

Acta Materialia– Received 22 March 2006; received in revised form 2 August 2006; accepted 7 August 2006.

above their equilibrium composition, which is a result of kinetically trapped Cr atoms for aging times up to 64 h [3].

Acknowledgements. This research is supported by the National Science Foundation, Division of Materials Research, under contract DMR-0241928. CKS received partial support from an NSF graduate research fellowship, a W. P. Murphy Fellowship, and a Northwestern University terminal year fellowship. We extend our gratitude to Dr. K. E. Yoon for some experimental results, Dr. T. F. Kelly, Imago Scientific Instruments, for use of a *LEAP* tomograph prior to our acquisition of this instrument, Prof. P. W. Voorhees for useful discussions, Dr. C. E. Campbell for diffusivity calculations, and Research Prof. G. Ghosh and Dr. N. Dupin for thermodynamic calculations employing *ThermoCalc*.

Acta Materialia– Received 22 March 2006; received in revised form 2 August 2006; accepted 7 August 2006.

References

[1] Sudbrack CK, Noebe RD, and Seidman DN, Phys. Rev. B 2006; 73: 212101.
[2] Sudbrack CK, Yoon KE, Noebe RD, and Seidman DN, Acta Mater. 2006; 54: 3199.
[3] Sudbrack CK, Noebe RD, and Seidman DN. In: Solid-Solid Phase Transformations in Inorganic Materials 2005, vol. 2. Howe JM, Laughlin DE, Lee JK, Srolovitz DJ, and Dahmen U (eds.). Phoenix, AZ: The Minerals, Metals & Materials Society; 2005, p. 543.
[4] Sudbrack CK, Yoon KY, Mao Z, Noebe RD, Isheim D, and Seidman DN. In: Electron Microscopy: Its Role in Materials Science, Weertman JR, Fine ME, Faber KT, King W, and Liaw P (eds.). Warrendale, PA: The Minerals, Metals & Materials Society; 2003, p. 43.
[5] Schmuck C, Caron P, Hauet A, and Blavette D, Philos. Mag. A 1997; 76: 527.
[6] Pareige C, Soisson F, Martin G, and Blavette D, Acta Mater. 1999; 47: 1889.
[7] Zener C, J. Appl. Phys. 1949; 20: 950.
[8] Ham FS, Phys. Chem. Solids 1958; 6: 335.
[9] Ratke L and Voorhees PW, Growth and Coarsening. Berlin: Springer-Verlag; 2002.
[10] Swalin RA, Thermodynamics in Solids. New York: John Wiley; 1972.
[11] Kuehmann CJ and Voorhees PW, Metall. Mater. Trans. 1996; 27A: 937.
[12] Umantsev A and Olson GB, Scr. Metall. 1993; 29: 1135.
[13] Engström A and Ågren J, Z. Metallk. 1996; 87: 92.
[14] Sudbrack CK, Ph. D. Thesis, Northwestern University, 2004.
http://arc.nucapt.northwestern.edu/refbase/show.php?record=16
[15] Lifshitz IM and Slyozov VV, J. Phys. Chem. Solids 1961; 19: 35.
[16] Wagner C, Z. Elektrochem. 1961; 65: 581.
[17] Ben Israel DH and Fine ME, Acta Metall. 1963; 11: 1051.
[18] Ardell AJ, Acta Metall. 1967; 15: 1772.
[19] Ardell AJ, Acta Metall. 1968; 16: 511.
[20] Wendt H and Haasen P, Acta metall. 1983; 31: 1649.
[21] Marquis EA and Seidman DN, Acta Mater. 2005; 53: 4259.
[22] Fuller CB, Murray JL, and Seidman DN, Acta Mater. 2005; 53: 5401; Fuller CB, Ph. D. Thesis, Northwestern University, 2003.
http://arc.nucapt.northwestern.edu/refbase/show.php?record=147
[23] Yoon KE, Ph. D. Thesis, Northwestern University, 2004.
http://arc.nucapt.northwestern.edu/refbase/show.php?record=15
[24] Campbell CE. Personal communication, 2003.
[25] Kelly TF, Camus PP, Larson DJ, Holzman LM, and Bajikar SS, Ultramicroscopy 1996; 62: 29.
[26] Fährmann M, Fährmann E, Pollock TM, and Johnson WC, Metall. Mater. Trans. 1997; 28A: 1943.
[27] Marquis EA, Ph. D. Thesis, Northwestern University, 2002.
http://arc.nucapt.northwestern.edu/refbase/show.php?record=151
[28] Dupin N, Ansara I, and Sundman B, Calphad 2001; 25: 279.
[29] Saunders N. In: Superalloys 1996, Kissinger JD, Deye DJ, Anton DL, Cetel AD, Nathal MV, Pollock TM, and Woodford DA (eds.). Warrendale, PA: The Minerals, Metals & Materials Society; 1996, p. 101.

Acta Materialia– Received 22 March 2006; received in revised form 2 August 2006; accepted 7 August 2006.

[30] Hellman OC, Blatz du Rivage JB, Vandenbrouke J, and Seidman DN, Mater. Sci. Eng. A 2002; 327: 29.
[31] Hellman OC, Blatz du Rivage J, and Seidman DN, Ultramicroscopy 2003; 95: 199.
[32] Hellman OC, Vandenbroucke JA, Rüsing J, Isheim D, and Seidman DN, Micros. Microanal. 2000; 6: 437.
[33] Huang W and Chang YA, Intermetallics 1999; 7: 863.
[34] Sundman B, Jansson B, and Andersson J-O, CALPHAD 1985; 9: 153.
[35] Voorhees PW, Annu. Rev. Mater. Sci. 1992; 22: 197.
[36] Brailsford AD and Wynblatt P, Acta Metall. 1979; 27: 489.
[37] Taylor A and Floyd RW, J. Inst. Met. 1952-53; 81: 451.
[38] Cermak J and Rothova, Defect Diffus. Forum 2005; 237-240: 83.
[39] Minamino Y, Jung SB, Yamane T, and Hirao K, Metall. Trans. A 1992; 23: 2783.
[40] Campbell CE, Boettinger WJ, and Kattner UR, Acta Mater. 2002; 50: 775.

Acta Materialia– Received 22 March 2006; received in revised form 2 August 2006; accepted 7 August 2006.

Table 1. Temporal evolution of the mean γ'-precipitate radius, solute supersaturations in the γ-matrix, and solute supersaturations in the γ'-precipitates for Ni-5.2 Al-14.2 Cr at.% aged at 873 K as determined by APT.

t (h)	$\langle R \rangle \pm \sigma$ (nm)	$\Delta C^{\gamma}_{Al} \pm \sigma$ (at.%)	$\Delta C^{\gamma}_{Cr} \pm \sigma$ (at.%)	$\Delta C^{\gamma'}_{Al} \pm \sigma$ (at.%)	$\Delta C^{\gamma'}_{Cr} \pm \sigma$ (at.%)
0.167	0.74 ± 0.24	2.06 ± 0.03	-1.39 ± 0.06	2.4 ± 1.3	2.9 ± 1.0
0.25	0.75 ± 0.14	1.94 ± 0.03	-1.41 ± 0.06	1.6 ± 0.5	2.4 ± 0.4
1	0.89 ± 0.14	1.62 ± 0.04	-1.25 ± 0.06	1.11 ± 0.32	2.03 ± 0.26
4	1.27 ± 0.21	0.84 ± 0.04	-0.59 ± 0.08	0.96 ± 0.24	1.25 ± 0.17
16	2.1 ± 0.4	0.48 ± 0.025	-0.33 ± 0.05	0.50 ± 0.16	0.56 ± 0.11
64	2.8 ± 0.6	0.32 ± 0.028	-0.28 ± 0.06	0.48 ± 0.18	0.39 ± 0.12
256	4.1 ± 0.8	0.17 ± 0.025	-0.14 ± 0.06	0.27 ± 0.14	0.31 ± 0.10
1024	7.7 ± 3.3	0.14 ± 0.028	-0.04 ± 0.06	0.01 ± 0.18	0.14 ± 0.13

Table 2. Compositional coarsening rate constants (κ_i^{KV}) determined from Figures 3 and 5 in the γ-matrix and γ'-precipitates for Ni-5.2 Al-14.2 Cr at.% aged at 873 K as measured by APT.

	Ni	Al	Cr
Measured coarsening rate constants for γ-matrix far-field composition, (at.% $s^{1/3}$)	-5 ± 5	18.6 ± 2.2	-14 ± 5
Measured coarsening rate constants for γ'-precipitates' interior composition (at.% $s^{1/3}$)	-48 ± 13	22 ± 11	26 ± 8

Acta Materialia– Received 22 March 2006; received in revised form 2 August 2006; accepted 7 August 2006.

Table 3. A comparison of APT measurements and quantities obtained by CALPHAD thermodynamic assessments for Ni-5.2 Al-14.2 Cr at.% aged at 873 K

	Ni	Al	Cr
Equilibrium volume fraction determined by lever-rule calculation with measured concentrations[a] (%)	15.6 ± 4.3	15.6 ± 0.9	15.5 ± 1.9
Measured volume fraction from APT images of specimens aged for 1024 h (%) [2]		15.6 ± 6.4	
Calculated equilibrium volume fraction (%) [33]		7.49	
Calculated equilibrium volume fraction (%) [28]		12.34	
Calculated equilibrium volume fraction (%) [29]		12.83	
Measured critical γ'-nucleus composition[b] (at.%) [2]	72.4 ± 1.1	18.3 ± 0.9	9.3 ± 0.7
Calculated critical γ'-nucleus composition (at.%) [28]	75.36	16.43	8.21
Calculated critical γ'-nucleus composition (at.%) [29]	74.91	17.40	7.69
Measured equilibrium composition of γ'-precipitates (at.%)	76.53 ± 0.25	16.69 ± 0.22	6.77 ± 0.15
Calculated equilibrium composition of γ'-precipitates (at.%) [28]	75.59	14.55	9.57
Calculated equilibrium composition of γ'-precipitates (at.%) [29]	74.97	16.21	8.82
Measured equilibrium composition of γ-matrix (at.%)	81.26 ± 0.09	3.13 ± 0.04	15.61 ± 0.09
Calculated equilibrium composition of γ-matrix (at.%) [28]	81.17	3.93	14.90
Calculated equilibrium composition of γ-matrix (at.%) [29]	81.34	3.62	15.04

[a] ϕ_{LR}^{eq} is calculated using the lever-rule, $\phi_{LR}^{eq} = \left(C_i^{\gamma,eq} - C_i^{o}\right)/\left(C_i^{\gamma,eq} - C_i^{\gamma',eq}\right)$

[b] This estimation is based on an average composition over the *total* distribution of γ'-precipitates where stationary-state nucleation dominates (t = 0.167–0.25 h), including overcritical γ'-nuclei, and is therefore a lower bound [2].

Acta Materialia– Received 22 March 2006; received in revised form 2 August 2006; accepted 7 August 2006.

Table 4. Curvatures in the molar Gibbs free-energy ($G^{\alpha}_{,ij}$) surface of a given phase (α) evaluated at the equilibrium composition with respect to components *i* and *j* obtained from ideal solution theory and CALPHAD thermodynamic assessments.

$G^{\alpha}_{,ij}$	Ideal Solution[a] (J mol^{-1})	Dupin et al. database [28][b,d] (J mol^{-1})	Saunders database [29][c,e] (J mol^{-1})
$G^{\gamma}_{,AlAl}$	242,383.30	365,962.25	336,512.41
$G^{\gamma}_{,AlCr}$	8,932.48	113,606.62	99,076.303
$G^{\gamma}_{,CrCr}$	55,443.18	117,511.87	117,229.52
$G^{\gamma'}_{,AlAl}$	–	359,893.91	1,259,600.1
$G^{\gamma'}_{,AlCr}$	–	334,701.72	968,769.9
$G^{\gamma'}_{,CrCr}$	–	491,645.8	1,010,737.9

[a] Ideal solution: $G^{\gamma}_{,AlAl} = R_g T(1 - C^{\gamma,eq}_{Cr})/(C^{\gamma,eq}_{Al} \cdot C^{\gamma,eq}_{Ni})$, $G^{\gamma}_{,CrCr} = R_g T(1 - C^{\gamma,eq}_{Al})/(C^{\gamma,eq}_{Cr} \cdot C^{\gamma,eq}_{Ni})$, and $G^{\gamma}_{,AlCr} = R_g T / C^{\gamma,eq}_{Ni}$ evaluated at the equilibrium composition determined by APT.

[b] Calculated equilibrium γ-composition of 0.0393 at. fr. Al and 0.1490 at. fr. Cr [28]

[c] Calculated equilibrium γ-composition of 0.0362 at. fr. Al and 0.1504 at. fr. Cr [29]

[d] Calculated equilibrium γ'-composition of 0.1455 at. fr. Al and 0.0957 at. fr. Cr [28]

[e] Calculated equilibrium γ'-composition of 0.1621 at. fr. Al and 0.0882 at. fr. Cr [29]

Acta Materialia– Received 22 March 2006; received in revised form 2 August 2006; accepted 7 August 2006.

Table 5. Free-energy of the γ/γ' interfaces, $\sigma_i^{\gamma/\gamma'}$, at 873 K in Ni-5.2 Al-14.2 Cr at.% calculated from the experimental values of the coarsening rate constants for the average precipitate radius and the supersaturation of solute species *i* employing Equation 13 with solution thermodynamics described by the ideal solution and CALPHAD databases in Table 4.

Thermodynamic models	$\sigma_{Al}^{\gamma/\gamma'}$ (mJ m^{-2})	$\sigma_{Cr}^{\gamma/\gamma'}$ (mJ m^{-2})	$<\sigma^{\gamma/\gamma'}>$ (mJ m^{-2})
Ideal solution theory	21.1 ± 5.2	23.8 ± 10.1	22 ± 7
Dupin et al. database [28]	22.3 ± 5.5	25.1 ± 10.7	23 ± 7
Saunders database [29]	21.4 ± 5.3	24.1 ± 10.3	22 ± 7

Table 6. A comparison of the calculated intrinsic solute *i* diffusivities, ${}^iD_{ii}^{fcc}$, and measured solute diffusivities D_{ii}^{eff} determined by Equation 14 and 14b.

Calculated intrinsic diffusivities[a] 10^{-21} (m^2 s^{-1})		Measured diffusivities[b] (effective) 10^{-21} (m^2 s^{-1})			
Campbell mobility database [40] utilizing Saunders database [29]			Ideal solution theory	Dupin et al. database [28]	Saunders database [29]
${}^iD_{AlAl}^{fcc}$	22.22	$D_{AlAl}^{eff,Al}$	1.6 ± 0.5	1.1 ± 0.4	1.2 ± 0.4
		$D_{AlAl}^{eff,Cr}$	1.4 ± 0.7	1.0 ± 0.5	1.1 ± 0.5
		$<D_{AlAl}^{eff}>$	1.5 ± 0.6	1.1 ± 0.4	1.2 ± 0.5
${}^iD_{CrCr}^{fcc}$	6.999	$<D_{CrCr}^{eff}>$	0.49 ± 0.19	0.34 ± 0.13	0.37 ± 0.15

[a] Intrinsic diffusivities [24], ${}^iD_{ii}^{fcc}$, for face-centered cubic Ni-5.24 Al-14.24 Cr at.% calculated with the thermodynamic database developed by Saunders [29] and the mobility database developed by Campbell [40] for Ni-based superalloys. The α_D is the ratio of ${}^iD_{AlAl}^{fcc}$ to ${}^iD_{CrCr}^{fcc}$.

[b] Measured solute (*j*) diffusivities, $D_{jj}^{eff,i}$, at 873 K in Ni-5.2 Al-14.2 Cr at.% calculated from the experimental values of the coarsening rate constants for the average precipitate radius, K^{KV}, and the supersaturation of solute species *i*, $\kappa_I^{\gamma,KV}$ (Table 2), employing Equation 14 using $\alpha_D = 3.175$ with solution thermodynamics described by the ideal solution and CALPHAD databases in Table 4.

Acta Materialia– Received 22 March 2006; received in revised form 2 August 2006; accepted 7 August 2006.

Figure captions

Figure 1. (a) A typical APT image for a Ni-5.2 Al-14.2 Cr at.% specimen at peak number density, $(3.2\pm0.6)\times10^{24}$ m^{-3}, after aging for 4 h at 873 K. This image shows that the fine-scale unifrom distribution of γ'-precipitates is a mixture individual spheroids, $\langle R\rangle = 1.27\pm0.21$ [2], and spheroids in various stages of coagulation and coalescence. Observed coalescence occurs primarily between pairs of γ'-precipitates, although coalescence between multiple γ'-precipitates is also observed (white arrow). The ~770,000 atoms contained within the 18x18x46 nm^3 analyzed volume are omitted to allow visualization of the γ/γ'-interfaces with gray 9 at.% Al isoconcentration surfaces.

Figure 2. The average far-field γ-matrix concentrations for Ni-5.2 Al-14.2 Cr at.% specimens aged at 873 K. The equilibrium phase composition ($C_i^{\gamma,eq}$) and coarsening rate constants ($\kappa_i^{\gamma,KV}$) are deduced by fitting the aging states in a quasi-stationary-state ($t \geq 16$ h) to Equation 4. The solid lines denote the fitting, while the dashed lines mark the continuation of the fit to shorter aging times.

Figure 3. The average concentrations in the interior of the γ'-precipitates for Ni-5.2 Al-14.2 Cr at.% specimens aged at 873 K. The equilibrium phase composition ($C_i^{\gamma',eq}$) and coarsening rate constants ($\kappa_i^{\gamma',KV}$) are deduced by fitting the aging ($t \geq 4$ h) to Equation 5. The solid lines denote the fitting, while the dashed lines mark the continuation of the fit to shorter aging times.

Figure 4. Partial isothermal section of the Ni-rich corner of the Ni-Al-Cr phase diagram at 873 K calculated utilizing *ThermoCalc* [34], employing Dupin et al.'s [28] and Saunders' [29] thermodynamic databases. APT measurements of γ'-precipitate and γ-matrix compositions as they evolve temporally are marked with open diamonds and triangles, respectively. Note well that the calculated phase boundaries differ from the experimentally determined points on the solvus lines. Calculated phase diagram courtesy of Research Prof. Gautam Ghosh and Dr. Natalie Dupin.

Figure 5. For γ'-precipitation in Ni-5.2 Al-14.2 Cr at.%, a double logarithmic plot of the second term in the Gibbs-Thomson relationship (Equation 15), which describes the Al supersaturation in the γ'-phase, was calculated from the measured compositions, calculated [28,29] free-energy curvatures of both phases (Table 4), and effective diffusivities (Table 6) versus $\langle R\rangle$. The power-law relationships marked with the solid (Saunders) and dashed (Dupin et al.) lines are the best-

Acta Materialia– Received 22 March 2006; received in revised form 2 August 2006; accepted 7 August 2006.

fits to the data, and are added to the first term to obtain the database predictions for the Gibbs-Thomson relationships in Figure 6.

Figure 6. Supersaturation of Al within the γ'-precipitates, as determined by APT for Ni-5.2 Al-14.2 Cr at.% aged at 873 K (Table 1), are compared to the Gibbs-Thomson relationship derived by Kuehmann and Voorhees for a ternary alloy (Equation 15) [11] using the thermodynamic assessments of Dupin et al. [28] and Saunders [29]. The Dupin and Saunders databases calculate similar curvatures in the Gibbs free-energy surface for the γ-phase, yielding almost identical values for the calculated interfacial free-energy, $\sigma^{\gamma/\gamma'}$ (Table 5). For the γ'-phase, however, the Saunders database predicts larger curvatures in the free-energy surface than the Dupin et al. database, leading to a shift in supersaturation to lower values.

Figure 7. Supersaturation of Cr within the γ'-precipitates, (a) as determined by APT for Ni-5.2 Al-14.2 Cr at.% aged at 873 K (Table 1), are compared to (b) the 1st term of the Gibbs-Thomson relationship derived by Kuehmann and Voorhees for a ternary alloy (Equation 15) [11] using the thermodynamic assessments of Dupin et al. [28] and Saunders [29]. Although these assesments predict that the Cr supersaturation within the γ'-precipitates increases, a decay is observed experimentally. In the quasi-stationary state ($t \geq 16$ h), a temporal power-law dependence of –1 is observed. The deviation from this dependence at shorter aging times may result from a nonnegligble contribution from the second term of the Gibbs-Thomson relationship (Equation 15).

Acta Materialia– Received 22 March 2006; received in revised form 2 August 2006; accepted 7 August 2006.

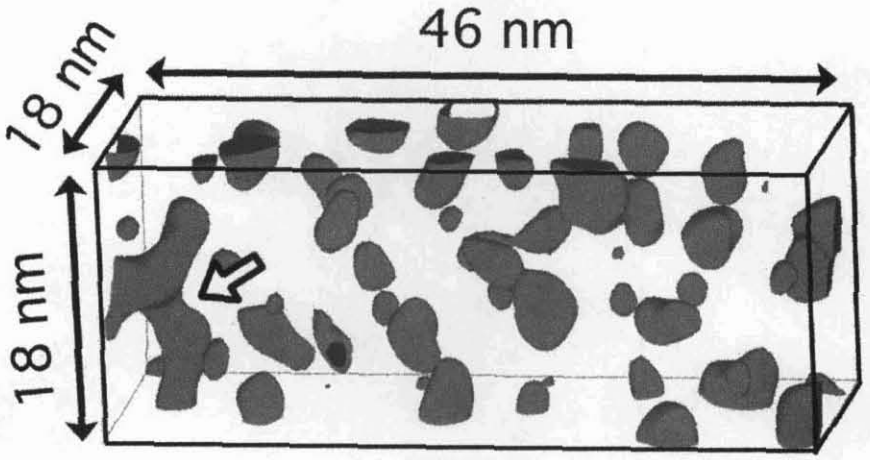

Figure 1

Acta Materialia– Received 22 March 2006; received in revised form 2 August 2006; accepted 7 August 2006.

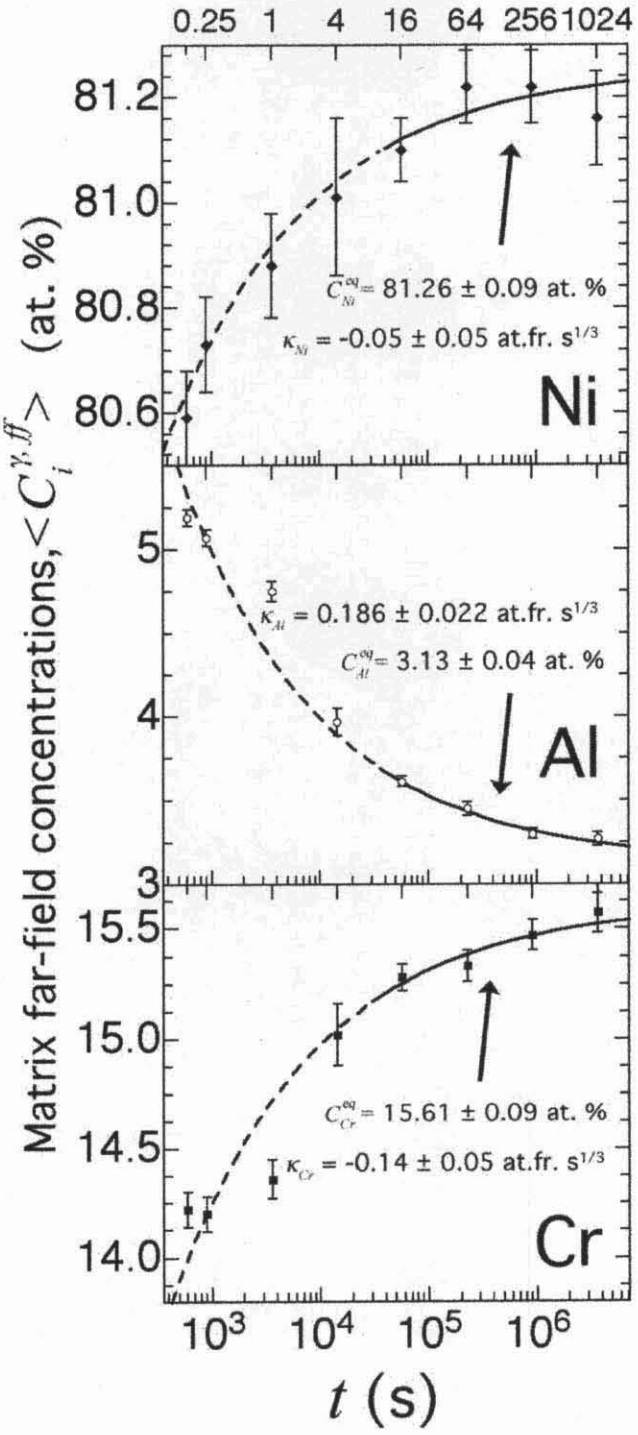

Figure 2

Acta Materialia– Received 22 March 2006; received in revised form 2 August 2006; accepted 7 August 2006.

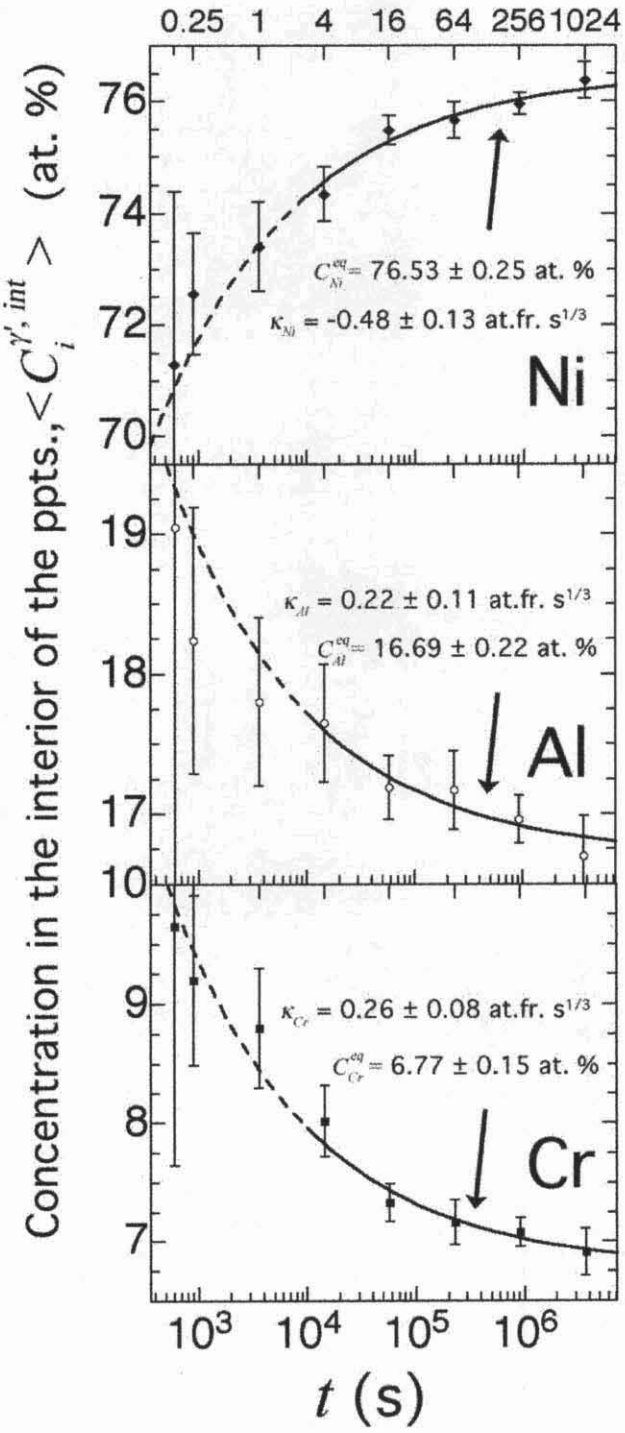

Figure 3

Acta Materialia– Received 22 March 2006; received in revised form 2 August 2006; accepted 7 August 2006.

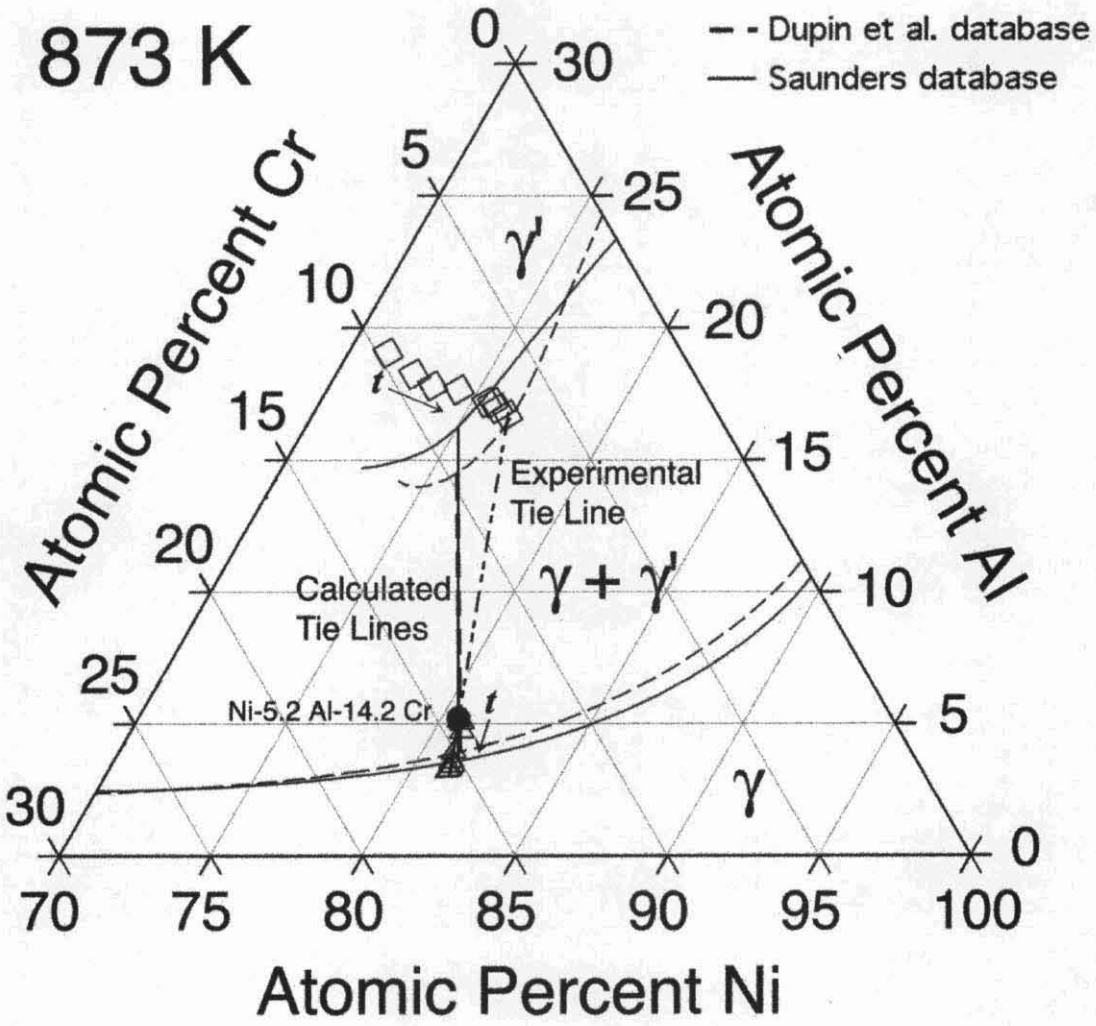

Figure 4

Acta Materialia– Received 22 March 2006; received in revised form 2 August 2006; accepted 7 August 2006.

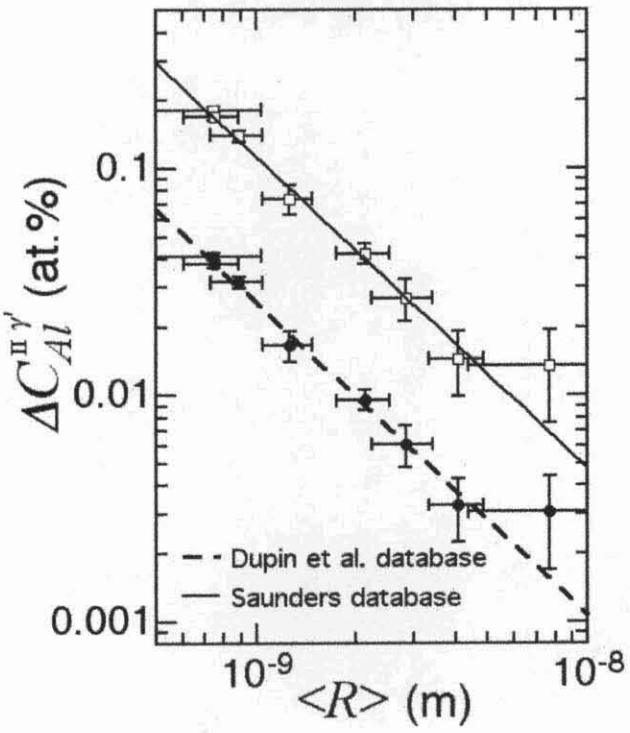

Figure 5

Acta Materialia– Received 22 March 2006; received in revised form 2 August 2006; accepted 7 August 2006.

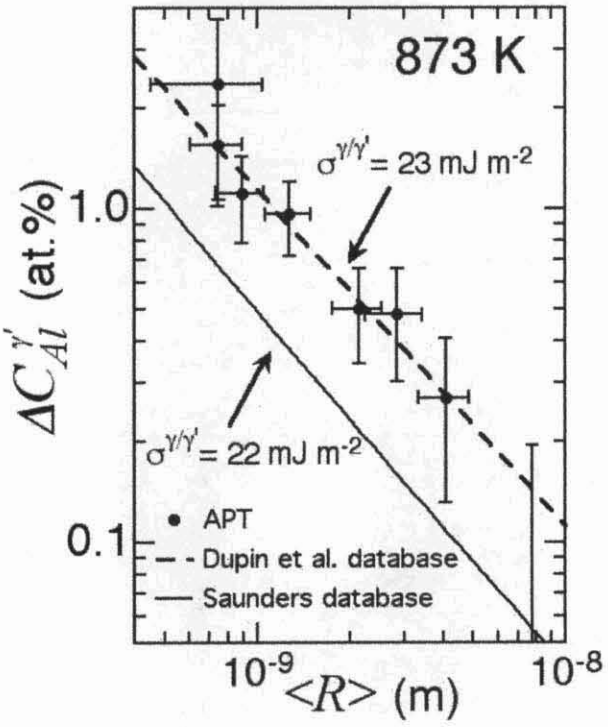

Figure 6

Acta Materialia– Received 22 March 2006; received in revised form 2 August 2006; accepted 7 August 2006.

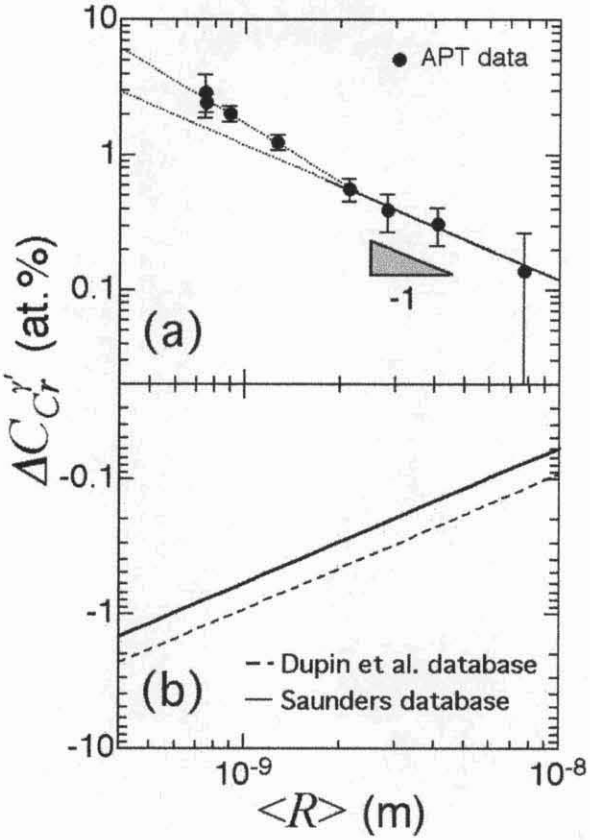

Figure 7